Surfaces and Interfaces 29 (2022) 101711

Contents lists available at ScienceDirect

Surfaces and Interfaces

journal homepage: www.sciencedirect.com/journal/surfaces-and-interfaces

Role of surface functional groups to superconductivity in Nb_2C-MXene: Experiments and density functional theory calculations

Kai Wang [a,1], Haolin Jin [a,1], Hongye Li [a], Zhongquan Mao [a], Lingyun Tang [a], Dan Huang [b], Ji-Hai Liao [a,*], Jiang Zhang [a,*]

[a] Department of Physics, South China University of Technology, Guangzhou 510640, China
[b] MOE Key Laboratory of New Processing Technology for Non-ferrous Metals and Materials, Guangxi Key Laboratory of Processing for Non-ferrous Metals and Featured Materials and School of Physical Science and Technology, Guangxi University, Nanning 530004, China

ARTICLE INFO

Keywords:
MXenes
Superconductivity
Nb_2C-MXene
Density functional theory

ABSTRACT

The recently discovered surface-group-dependent superconductivity in Nb_2C-MXene fabricated by the molten salts method is attracting wide attention. However, regarding the superconductivity of Nb_2C-MXene with functional F groups (Nb_2CF_x), there were some conflicting results in experimental and theoretical studies. Herein, we systematically carried out experimental and theoretical investigations on the superconductivity in Nb_2C-MXene with the Cl functional group (Nb_2CCl_x) and Nb_2CF_x. The experimental results of the Meissner effect and zero resistivity have proved that Nb_2CCl_x is superconducting with the transition temperature (T_c) ~ 5.2 K. We extract its superconducting parameters from the temperature dependence of resistivity and the field dependence of the magnetization. The Ginzburg-Landau parameter κ_{GL} is estimated to be 2.41, indicating that Nb_2CCl_x is a typical type-II superconductor. Conversely, both magnetic and electrical transport measurements demonstrate that Nb_2CF_x is not superconducting. The first-principles density functional theory (DFT) calculations show that the T_c of Nb_2CCl_x is ~ 5.2 K, while Nb_2CF_x is dynamically unstable with imaginary frequency in phonon spectrum, which is in good agreement with the experimental results. Our studies not only are useful for clarifying the present inconsistency but also offer referential significance for future investigations on the superconductivity of MXenes.

1. Introduction

MXenes are generally referred as a new type of two-dimensional (2D) transition metal carbide, nitride and boride with chemical formula of $M_{n+1}X_nT_x$, where M represents transition metal, X represents carbon, nitrogen, or boron, $n = 1, 2, 3$, T is surface-linked F, OH, O, Cl, and other active functional groups [1–6]. With unique properties such as good electrical conductivity, magnetic properties, and thermoelectric properties, MXenes are quite useful in a large number of applications, including energy storage, optoelectronic, biomedical, electromagnetic shielding and photovoltaic [7–14].

In terms of superconductivity, α-Mo_2C crystal with the transition temperature (T_c) of 3.6 K was the first reported two-dimensional (2D) transition metal carbide, which showed observable characteristics of Berezinskii-Kosterlitz-Thouless transition [15,16]. But α-Mo_2C is different from the MXenes we mentioned above, it was grown using the chemical vapor deposition (CVD) technique, not etched from the MAX phase, so it has no functional group [17]. Although fewer superconductors of the MAX phase, such as Nb_2AlC (T_c ~ 0.44 K), Lu_2SnC (T_c ~ 5.2 K), Nb_2InC (T_c ~ 7.5 K) [18–20], were reported previously. It was only recently discovered that the Nb_2C-MXene with different functional groups (Nb_2CCl_2 (T_c ~ 6 K), Nb_2CS_2 (T_c ~ 6.4 K), Nb_2CSe (T_c ~ 4.5 K), and $Nb_2C(NH)$ (T_c ~ 7.1 K)) were superconducting, which were fabricated by performing substitution and elimination reactions in molten inorganic salts [21]. Besides, the superconducting parameter, such as H_{c2}, showed a strong dependence on the surface functional group, the H_{c2} of Nb_2CNH was nearly 3 times that of Nb_2CCl_2 [21], which suggested that surface groups played a crucial role to the superconductivity of Nb_2C MXene. Through the magnetic measurement, Nb_2C-MXene with the F functional group (Nb_2CF_x) etched by hydrofluoric acid (HF) was found to show the Meissner effect with the highest T_c of 12.5 K [22,23]. However, zero resistivity, which is identified as the most important

* Corresponding authors.
E-mail addresses: jhliao@scut.edu.cn (J.-H. Liao), jonney@scut.edu.cn (J. Zhang).
[1] These authors contributed equally to this work.

https://doi.org/10.1016/j.surfin.2021.101711
Received 7 November 2021; Received in revised form 22 December 2021; Accepted 28 December 2021
Available online 30 December 2021

evidence of superconductivity, was absent. The temperature dependence of resistivity for the pressed Nb_2CF_x pellet indicated a sharp increase with decreasing temperature [21], which is similar to the electrical properties of Nb_2CT_z-yLi thin film [24]. Neither two transport experiments of Nb_2CF_x MXene did show the superconducting behavior. On the other hand, first-principle calculations on intrinsic Nb_2C showed no superconductivity [25]. Theoretical studies on both pristine and functionalized Nb_2C-MXene using the density functional theory (DFT) suspected that the possible reason for the superconductor with $T_c \sim$ 12.5 K observed is Nb_2CO_2 rather than Nb_2CF_x [26].

To clarify the above confused and inconsistent results and in-depth understand the superconductivity of Nb_2C-MXene, we have systematically studied the superconductivity of Nb_2CCl_x and Nb_2CF_x through experiments and theoretical calculations. We prepared Nb_2CCl_x and Nb_2CF_x respectively and studied the magnetic and electrical transport properties as a function of temperature. Combined with the theoretical computations, our results show that different functional groups do have a great influence on the superconductivity of Nb_2C-MXene, when the linked functional group is Cl the superconducting performance is better, and when the linked functional group is F, there is no superconductivity was observed.

2. Experimental and characterization

2.1. Preparation of Nb_2CF_x and Nb_2CCl_x

The materials used here include hydrochloric acid solution (wt 38%), lithium fluoride powder (LiF, purity 97%), hydrofluoric acid solution (wt 40%), niobium aluminum carbon powder (Nb_2AlC, purity 97%, 400 mesh), anhydrous cadmium chloride powder ($CdCl_2$, purity 99%), deionized water and anhydrous ethanol.

For Nb_2CF_x, we employed two methods to strip the Nb_2AlC MAX phase. Hydrothermal method [27]: Firstly, 2 g lithium fluoride powder and 40 ml hydrochloric acid solution were mixed and sonicated for 30 mins. Then 0.5 g Nb_2AlC powder was added to the mixed solution. The solution was sealed in an autoclave and heated at 120 °C for 36 h. HF etching method: 0.5 g Nb_2AlC powder was added to 40 ml of hydrofluoric acid solution and reacted for 96 h in a tetrafluoroethylene reactor at 60 °C.

For Nb_2CCl_x, we used the molten salt method to etch Nb_2AlC [21]. Firstly, the $CdCl_2$ powder and the Nb_2AlC powder were mixed according to a molar ratio of 10:1 and ball milled for 12 h. The mixture was put in a corundum crucible and kept at 300 °C for 8 h in a tube furnace under the flow of argon gas (mixed 5% hydrogen), and then reacted at 750 °C for 36 h. After the completion of the reaction, the obtained products were stirred and washed with hydrochloric acid for 12 h.

We adopted the same post-processing process to get the MXene products. The reacted solution was centrifuged at 7000 rpm for 5 min and washed with deionized water several times ultrasonically until the pH of the supernatant reached 7. The precipitate was taken out from the centrifuge tube with ethanol and dried at 55 °C under vacuum for 12 h to obtain Nb_2C-MXene powders.

2.2. Characterization

The structure and morphology of Nb_2C-MXene were characterized using scanning electron microscopy (SEM, Gemni500) and X-ray diffraction (XRD, Bruker D8 ADVANCE). DC and AC magnetic susceptibility, as well as resistivity, were measured by the Physical Property Measurement System (PPMS Evercoll II, Quantum Design) in the temperature range of 2–300 K with a vibrating sample magnetometer and electrical transport option. The powders samples were pressed into a circular disk with a diameter of 8 mm and a thickness of 1.5 mm, and the standard four-wire method was used to measure resistivity. The chemical composition of Nb_2C-MXene was defined by an energy dispersive X-ray (EDX, OXFORD X-Max^N) and X-ray photoelectron spectrometer (XPS, Thermo Fisher Scientific K-Alpha).

2.3. Calculation details

Our calculations are based on DFT used in the QUANTUM-ESPRESSO package [28]. We use ultra-soft pseudopotential with generalized gradient approximation (GGA) in Perdew-Burke-Ernzerhof (PBE) format for exchange correlation potential [29,30]. The *4 s, 5 s, 4p*, and *4d* electrons of Nb, the *2 s* and *2p* electrons of C and F, and the *3 s* and 3*p* electrons of Cl are considered as valence electrons.The threshold energy of a plane wave is defined as 680 eV (50 Ry), and all crystal structures are completely relaxed until the Herman-Feynman force on each atom is less than 2.57×10^{-4} eV/Å (10^{-5} Ry/Bohr). A Methfessel-Paxton [31] smearing of 0.272 eV (0.02 Ry) was used for the corresponding electronic self-consistent cycles. Phonon frequencies and EPC parameter λ were calculated with the phonon wave-vector meshes of $6 \times 6 \times 1$ and the denser k meshes of $24 \times 24 \times 4$.

3. Results and discussion

3.1. Structure and morphology

The XRD patterns of Nb_2CF_x MXene obtained from the hydrothermal method and Nb_2CCl_x are illustrated in Fig. 1a and b. These two profiles can be indexed to *P63/mmc* with lattice parameters of $a = 3.134$ Å, $c = 23.68$ Å and $a = 3.162$ Å, $c = 17.6551$ Å, respectively. From the comparison of the XRD pattern of the Nb_2AlC MAX phase (Fig. S1a), we can find that the (102) peak of the MAX phase near 39° have disappeared. At the same time, the shift of the (002) peak to a low angle proves that the layer spacing has increased significantly after etching. The position of the (002) diffraction peak of Nb_2CF_x has changed from 12.8° to 7.37° and the D-spacing has increased from 6.91 Å to 11.98 Å. Meanwhile, the position of the (002) diffraction peak of Nb_2CCl_x has changed to 10.03° and the D-spacing has increased to 8.82 Å. The shift of the (002) peak and the disappearance of the remaining peaks confirm the conversion of the MAX phase to the MXene phase after etching[22]. The SEM images of Nb_2CF_x and Nb_2CCl_x are illustrated in Fig. 1c and d. Both of the MXene products have a typical layered structure. XRD pattern and SEM image of Nb_2CF_x obtained from HF etching present a similar structure (Fig. S1b, c).

We used XPS and EDX to characterize the contents of F and Cl in Nb_2CF_x and Nb_2CCl_x as shown in Fig. S2. The existence of F and Cl is evidenced by the main peak at 685.6 eV and 199.5 eV, respectively. It can be seen that Al is basically etched away from the results of the elemental composition measured by EDX (Table S2). The content of F and Cl are displayed at the same time in Tables S2 and S3. It should be noted that carbon pollution is inevitable in XPS and EDX measurement, so the content of C in Tables S2 and S3 is for reference only. Based on the structural and elemental analysis results, we successfully prepared Nb_2CF_x and Nb_2CCl_x MXenes.

3.2. Magnetic and electrical measurements

The Meissner effect and zero resistivity are the two most basic and prerequisite features of superconductivity. To study the effect of two different functional groups on the superconductivity of Nb_2C-MXene, we measured the dependent curves of magnetization with temperature on Nb_2CF_x and Nb_2CCl_x. The powder sample was put in a plastic capsule with a linear diamagnetic background to measure its magnetization. Fig. 2a shows the magnetization versus temperature of Nb_2CF_x synthesized from the hydrothermal method measured at 20 Oe, which does not exhibit superconducting behavior. The temperature dependence of the magnetization of Nb_2CCl_x with zero-field cooling (ZFC) and field cooling (FC) at 20 Oe is illustrated in Fig. 2b. It is apparent that the magnetization of Nb_2CCl_x has a sudden diamagnetic drop at 5.2 K, and the ZFC and FC curves are bifurcated at this temperature. According to the

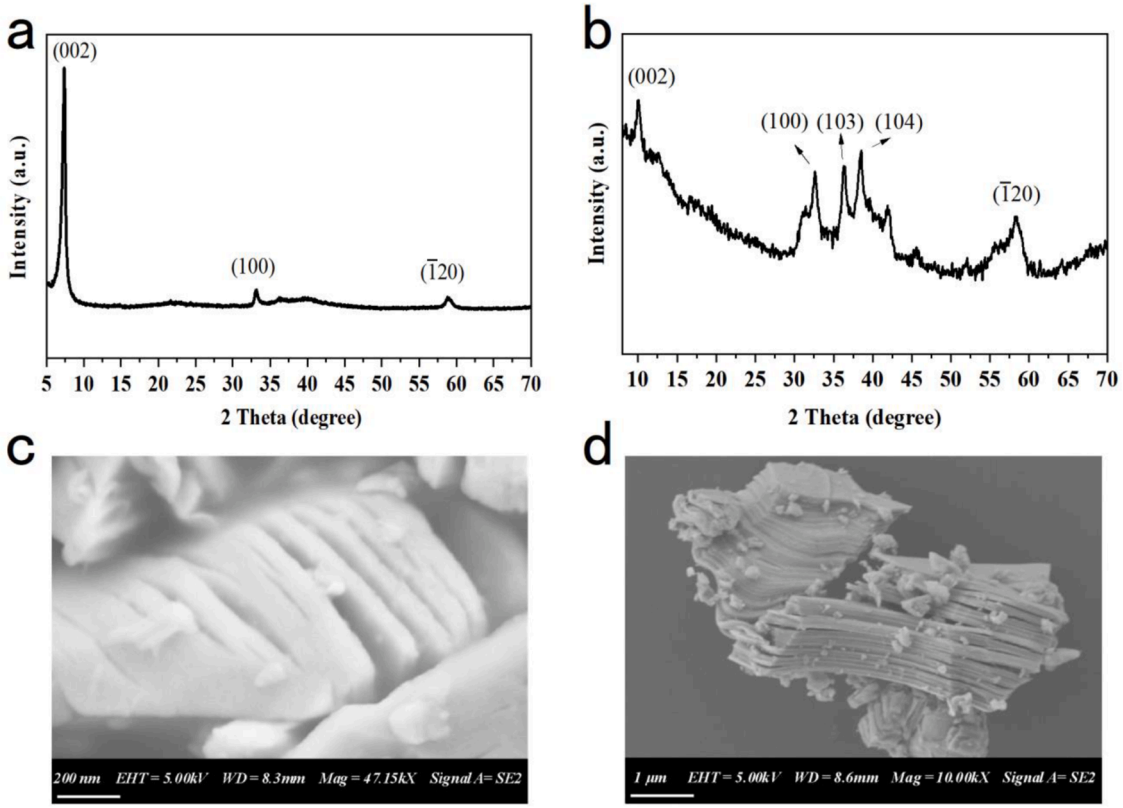

Fig. 1. (a) The XRD pattern of Nb_2CF_x prepared by the hydrothermal method, (b) The XRD pattern of the prepared Nb_2CCl_x, The SEM images of (c) Nb_2CF_x and (d) Nb_2CCl_x.

Meissner effect, it can be judged that the Nb_2CCl_x is superconducting, and the T_c is ~ 5.2 K, comparable to the value of 6 K reported by Kamysbayev et al. [21]. Given the crystallographic density is 5.3 g/cm^3, from the magnetic susceptibility at 2 K of −0.00342 emu/(g•Oe), the shielding volume fraction is estimated as 22.8%.

Our experimental results show that Nb_2CF_x is not superconducting, which is converse from the recent reports [22,23]. It should be pointed out that the diamagnetic shielding volume fraction estimated by their magnetic measurements was only about 0.12%, and the zero resistivity (ρ) data of the superconductor was absent. To further study the physical properties of Nb_2CF_x, it is necessary to measure the resistivity curves with temperature. Fig. 2c illustrates the temperature-dependent resistivity of Nb_2CF_x prepared by the hydrothermal method. When the temperature drops below 100 K, the resistivity increases abruptly, and no superconductivity was detected even the temperature down to 2 K. We also measured the magnetization and resistivity of Nb_2CF_x etched by HF, and the result was similar to that taken from the hydrothermal method, there was no sign of superconductivity (Fig. S3).

As shown in Fig. 2d, the resistivity of Nb_2CCl_x increases by about 42% in the temperature range of 300 K to 8 K, indicating that Nb_2CCl_x behaves more like non-metallic. When the temperature is below 6 K, the resistivity drops suddenly and sharply and then stabilizes to zero after 4 K. This provides very firm evidence for the existence of superconductivity of Nb_2CCl_x. The inset of Fig. 2d manifests an enlarged view of the ρ - T curve. We define T_c as taking the intersection of the tangent of the two lines of the normal state and the dropping state. It can be seen from the illustration that T_c is ~ 5.2 K, which is similar to data obtained from the magnetic measurement (Fig. 2b).

The AC magnetic susceptibility can provide further information for superconductivity. The real component $\chi_{ac}^{'}$ of the ac susceptibility reveals the diamagnetic shielding, and the imaginary part $\chi_{ac}^{''}$ is a measure of the absorption of energy as the sample transitions between the normal to the superconducting states. As shown in Fig. 3, both of them change abruptly at around 5.2 K. The transition temperature is the same as the temperature measured by the ZFC and FC curves. Combining the Meissner effect, the measurement of AC susceptibility and resistivity, we are convinced that Nb_2CCl_x is superconducting with T_c of 5.2 K.

3.3. *Superconducting state parameters of Nb_2CCl_x*

Generally, we can determine the type of superconductor by the Ginzburg-Landau parameterκ, which is calculated by the fitting upper critical field (H_{c2}) and lower critical field (H_{c1}) according to the Ginzburg-Landau theory. To figure out the H_{c2} and H_{c1} of Nb_2CCl_x, we measured superconductivity under the various magnetic field at different temperatures. Fig. 4 shows the curve of the resistivity versus temperature under different magnetic fields up to 2.8 T. As the magnetic field increases, the ρ-T curve shifts to a lower temperature, indicating that superconductivity is suppressed. At a temperature of 2 K, the superconductivity is still not destroyed when the magnetic field is increased to 2.8 T. The ρ-T curve under different magnetic fields can determine the superconducting parameter H_{c2}. The T_c used to determine H_{c2} is the same as the previous T_c criterion for resistivity measurement. The inset of Fig. 4 indicates the measured value of H_{c2} and the fitting curve (solid line) according to the Ginzburg-Landau equation [32]:

$$H_{c2}(T) = H_{c2}(0)\left[1 - (T/T_c)^2\right] \quad (1)$$

The obtained value of $H_{c2}(0)$ is 3.57 T.

Fig. 5 shows the magnetic fields dependence of magnetization in the temperature range of 2–4 K. Because there are some paramagnetic impurities in the tested samples, we have made background corrections to the data. The butterfly curves of hysteresis loops depict the typical characteristic of type-II superconductors. In the beginning, the magnetization decreases linearly until the magnetic field exceeds the lower critical field (H_{c1}). The inset of Fig. 5 presents the change of H_{c1} and H_{c2}

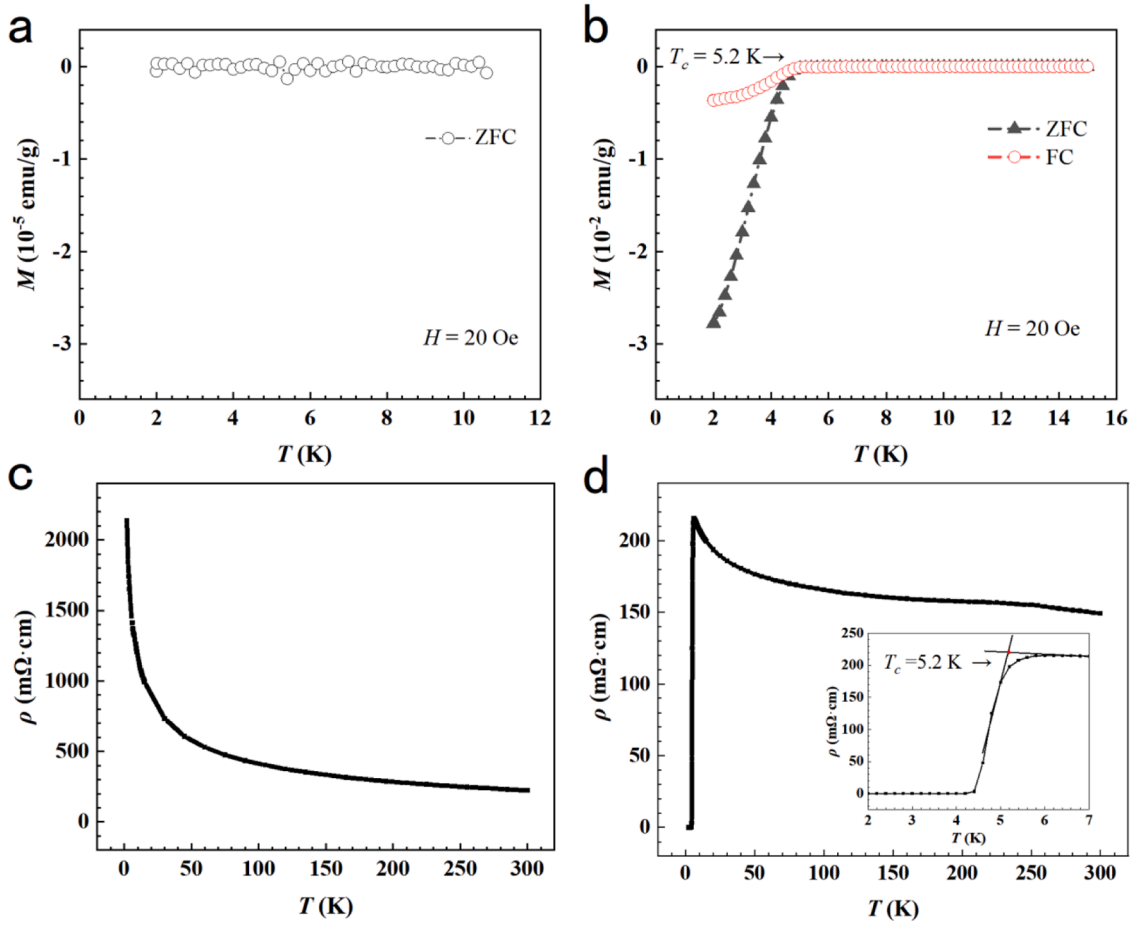

Fig. 2. (a) Temperature dependence of magnetization of Nb_2CF_x (Hydrothermally etched) under 20 Oe field, (b) FC and ZFC curves under 20 Oe field of Nb_2CCl_x, (c) Resistivity versus temperature curve of Nb_2CF_x (Hydrothermally etched), (d) Temperature dependence of resistivity of Nb_2CCl_x. The inset illustrates the data of the low-temperature section and how to define the T_c.

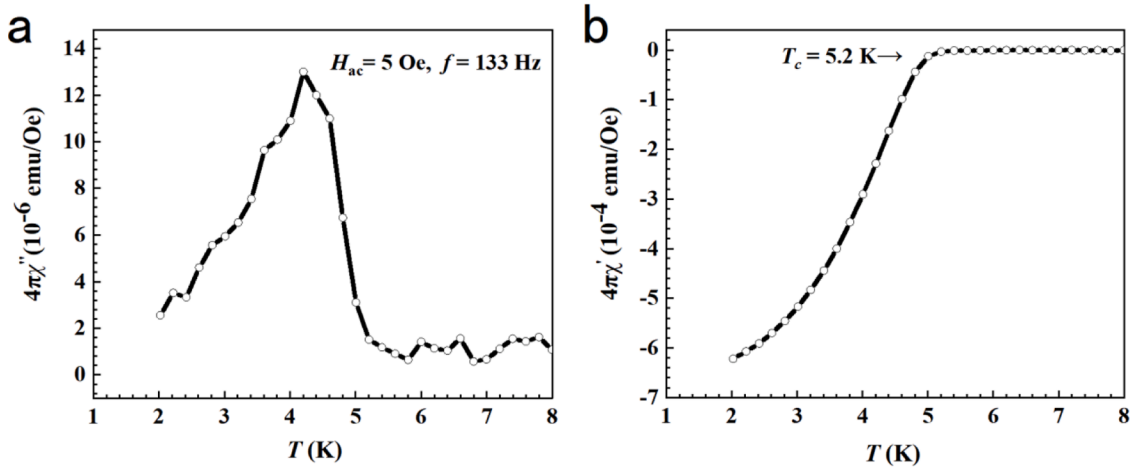

Fig. 3. (a) The imaginary magnetic susceptibility χ_{ac}'' and (b) The real magnetic susceptibility χ_{ac}' with temperature of Nb_2CCl_x, indicating a superconducting T_c of ~ 5.2 K. The harmonic magnetic field and frequency are 5 Oe and 133 Hz, respectively.

with temperature and the fitting curve (solid line) according to the Ginzburg-Landau equation:

$$H_{c2}(T) = H_{c2}(0)\left[1-(T/T_c)^2\right] \quad (2)$$

$$H_{c1}(T) = H_{c1}(0)\left[1-(T/T_c)^2\right] \quad (3)$$

The obtained values of $H_{c1}(0)$ and $H_{c2}(0)$ are 0.283 T and 3.3 T.

The coherence length ξ_{GL} and penetration depth λ_{GL} can be determined by the equation for the critical fields:

$$H_{c2}(0) = \frac{\Phi 0}{2\pi\xi_{GL}^2} \quad (4)$$

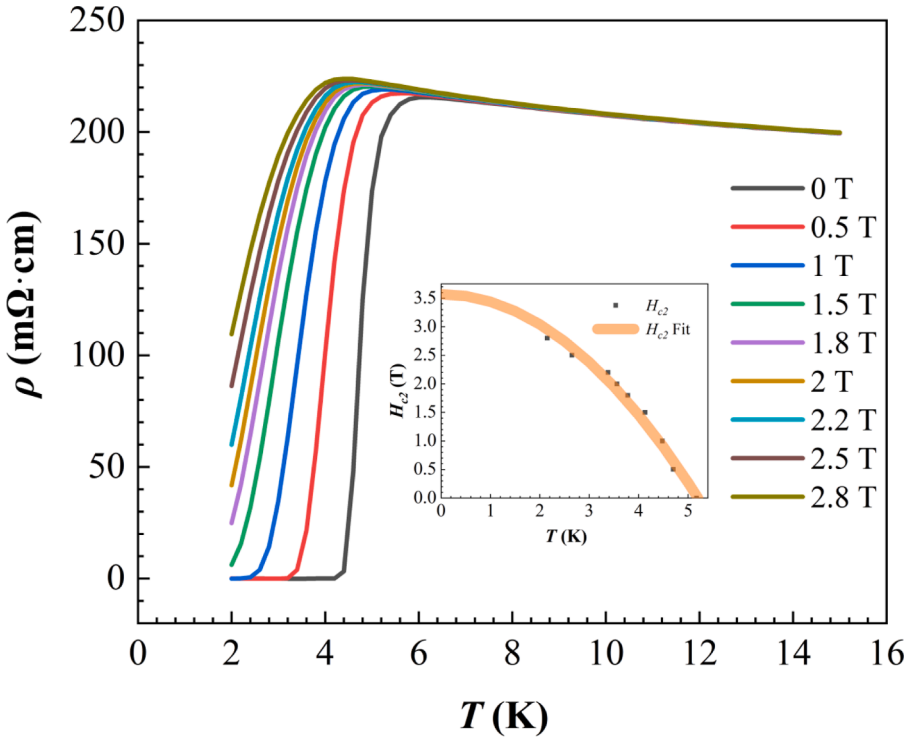

Fig. 4. Temperature dependence of resistivity at various magnetic fields from 0.0 to 2.8 T of Nb_2CCl_x. The inset illustration shows the experimental value of H_{c2} determined by the ρ - T curve and the fitted curve with the Ginzburg-Landau theory.

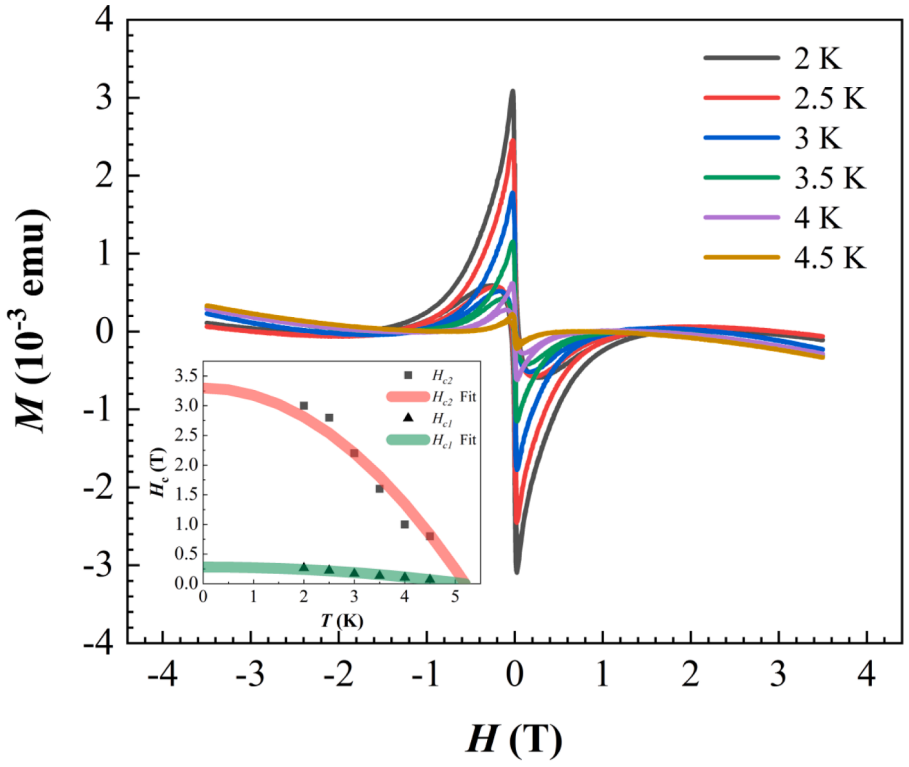

Fig. 5. Magnetization (M) dependence on the applied magnetic field (H) hysteresis loops measured at different temperatures of Nb_2CCl_x. The inset illustration shows the experimental value of H_{c1} and H_{c2} determined by the hysteresis curve and the fitted curve (solid line) with the Ginzburg-Landau theory.

$$H_{c1}(0) = \frac{\Phi 0}{4\pi\lambda_{GL}^{2}} \ln\frac{\lambda GL}{\xi GL} \quad (5)$$

Where $\Phi 0 = \frac{h}{2e}$ is the flux quantum, $Hc2(0)$ is the Ginzburg-Landau fitting data from the ρ-T curve. In this way, we obtained the coherence length ξGL=96.08 Å and penetration depth λGL=231.36 Å.

The superconducting thermodynamic critical field $H_c(0)$ can be

determined by the geometric mean of $H_{c1}(0)$ and $H_{c2}(0)$ as $H_c(0) = \sqrt{H_{c1}(0) \times H_{c2}(0)}$ [32], the calculated value is to be 0.97 T. According to Ginzburg-Landau theory, H_{c2} and H_c have the following relationship:$H_{c2} = \sqrt{2}\kappa_{GL}H_c$. Thus, the Ginzburg-Landau parameter κ_{GL} is estimated to be 2.41. This parameter also confirms that Nb_2CCl_x is a type-superconductor. The superconducting parameters of Nb_2CCl_x are summarized in Table 1.

3.4. The effect of structure and localization on superconductivity

Our experimental results clearly show that Nb_2CCl_x is superconducting while Nb_2CF_x is not. In addition to the different functional groups, it can be found from Figs.1a, b and S1 that the layer distances of the three samples are different. It is well established that annealing can reduce layer spacing of MXenes [33,34]. To verify whether the layer spacing has an effect on the superconductivity, we annealed Nb_2CF_x under a vacuum at 250 °C. It was shown that the interlayer spacing of Nb_2CF_x was reduced from 11.98 Å to 8.82 Å after annealing, which was similar to the value of Nb_2CCl_x. The XRD patterns before and after annealing are illustrated in Fig. S4a, only the (002) peak is shifted and no other impurities are introduced. However, magnetic measurement shows the annealed Nb_2CF_x sample is still not superconducting (Fig. S4b). Therefore, we confirm that the functional group is the main reason that affects the superconducting performance, not the layer spacing. Table S1 gives the different structural parameters of Nb_2CCl_x and Nb_2CF_x and annealed Nb_2CF_x.

From 10 K to 150 K, we found that the ρ-T curves of Nb_2CF_x and Nb_2CCl_x are very similar. This non-metallic behavior can be illuminated as the two-dimensional weak localization (WL) of charge carriers caused by the disorder. We fitted the resistivity data based on the function:

$$\rho = \frac{1}{\sigma 0 + a\, T^{\frac{1}{2}}} + b\, T^2 \tag{6}$$

where $\sigma_0 = 1/\rho_0$ is the residual conductivity, $aT^{1/2}$ is related to quantum correction from the electron-electron interaction, and the second term describes the high temperature part [35–39]. As shown in Fig. 6, this model describes the two experimental data very well ($R^2 = 0.99$) and give the fit parameters for Nb_2CF_x: $\sigma_0 = 1.364 \times 10^{-4}$ $m\Omega^{-1}\bullet cm^{-1}$, $a = 2.247 \times 10^{-4}$ $m\Omega^{-1}\bullet cm^{-1}\bullet K^{-1/2}$, and $b = -6.065 \times 10^{-4}$ $m\Omega\bullet cm\bullet K^{-2}$; and for Nb_2CCl_x: $\sigma_0 = 4.17 \times 10^{-3}$ $m\Omega^{-1}\bullet cm^{-1}$, $a = 2.15 \times 10^{-4}$ $m\Omega^{-1}\bullet cm^{-1}\bullet K^{-1/2}$, and $b = 6.55 \times 10^{-4}$ $m\Omega\bullet cm\bullet K^{-2}$. It should be noted that magnetoresistance measurements on Nb_2C-MXene etched by hydrofluoric acid also manifested similar weak localization behavior [40].

More importantly, parameter a is related to the disorder, which is enhanced with the increase of the disorder increases [41]. Meanwhile, the weak localization effect weakens electron-phonon interactions, that is to say, superconductivity is suppressed [42]. The parameter a follows the relation:

$$a = \lambda_F^4 \left(\frac{ne^2}{h}\right)^{3/2} \frac{(2m^*k_B)^{1/2}}{h} \sigma_0^{-1/2} \tag{7}$$

$$\lambda_F \propto N(E_F) \tag{8}$$

Table 1
Superconducting parameters of Nb_2CCl_x.

Parameter	Unit	Value
T_c	K	5.2
H_{c1}	T	0.28
H_{c2}	T	3.57
H_c	T	0.99
ξ_{GL}	Å	96.08
λ_{GL}	Å	231.36
κ_{GL}	—	2.41

The density of states on the Fermi surface ($N(E_F)$) directly affects the formation of Cooper pairs, which is the premise of superconductivity. Taking the obtained WL fitting parameters into formula (7), we draw a conclusion that λ_F of Nb_2CF_x is smaller than Nb_2CCl_x. Considering $N(E_F)$ is directly proportional to λ_F (formula (8)), $N(E_F)$ of Nb_2CCl_x is more than that of Nb_2CF_x. Our following theoretical calculations also support the conclusion. Thus, the functional group of Nb_2C-MXene will result in different extents of carriers localization and significantly change $N(E_F)$, which may be the main reason why Nb_2CCl_x is superconducting, whereas Nb_2CF_x is not.

3.5. Theoretical calculations

To get an insight into the superconductivity of Nb_2C-MXene, we performed DFT calculations using the QUANTUM-ESPRESSO package, which was widely used to compute the surface properties [43–46]. In order to reduce the computational cost, we adopted a structure nominally composed of Nb_2CCl_2 (Nb_2CF_2) [21], which was indexed to the space group $P6_3/mmc$ with optimized lattice constants $a = 3.33$ (3.20) Å and $c = 19.12$ (17.00) Å, respectively (Fig. 7a). Fig. 7b show the first Brillouin zone of Nb_2CCl_2 and the Highly symmetric paths Γ→K→M→A. This structure is dynamically stable, as no imaginary phonon frequency appears in the Brillouin zone (Fig. 7c). We calculate the T_c by using the McMillan-Allen-Dynes parameterized Eliashberg equation [47],

$$Tc = \frac{\omega_{\log}}{1.2} \exp\left(-\frac{1.04(1+\lambda)}{\lambda - \mu^*(1+0.62\lambda)}\right) \tag{9}$$

where $\omega_{\log}$ is the logarithmic averaged phonon frequency and λ is the total electron-phonon coupling constant.

Fig. S5 illustrates the range of T_c variation with Coulomb repulsion pseudopotential μ*. The calculated value of T_c decreases with increasing μ*. An estimated value of T_c is 5.3 K with $\mu^* = 0.1$, which is a reasonable value used widely in the literature [48–54]. The results show that Nb_2CCl_2 is a BCS superconductor. Phonon density of states (PHDOS) and Eliashberg function $\alpha^2F(\omega)$ for Nb_2CCl_2 are shown in Fig. 7d and 7e. Their peaks almost coincide. The densities of state of low frequency modes accounts for most of PHDOS. The low frequency vibration modes below 200 cm^{-1} induce the main electron-phonon coupling. The electron-phonon coupling constant λ is 0.63. Phonon softening has a great effect on superconductivity. The noticeable low frequency soft phonons at $\frac{1}{2}$ΓK with significant big linewidth (Fig. 7c) led to the peak of Eliashberg spectral function.

Rather, our calculations show that the Nb_2CF_2 with space group $P6_3/mmc$ is dynamically unstable. As shown in Fig. S6, the phonon mode with significant imaginary frequency at high symmetric point M indicates that the Nb_2CF_2 prefers to form ($2 \times 2 \times 1$) CDW phase than the normal phase. The calculated electronic structures show that the $N(E_F)$ of Nb_2CCl_2 of 3.2 states/eV/cell is larger than that of Nb_2CF_2 of 2.6 states/eV/cell (Figs. S7 and S8), which is consistent with our previous transport experimental analysis and may dominate whether or not superconductivity occurs. The present studies thus should give valuable insight into the precise ground state structure of Nb_2C-MXene and the surface-groups- dependent superconductivity.

4. Conclusion

In summary, the role of surface functional groups to superconductivity in Nb_2C-MXene has been investigated by experiments and DFT calculations. We have corroborated that Nb_2C-MXene with Cl functional group is superconducting and belongs to the type-II superconductor, while Nb_2CF_x with F functional group is not superconducting. The different functional groups of Nb_2C-MXene affect the carrier localization and significantly change the density of states on the Fermi surface, which may lead to superconductivity emergence or not. What needs illustration is that these two Nb_2C-MXenes were synthesized by different

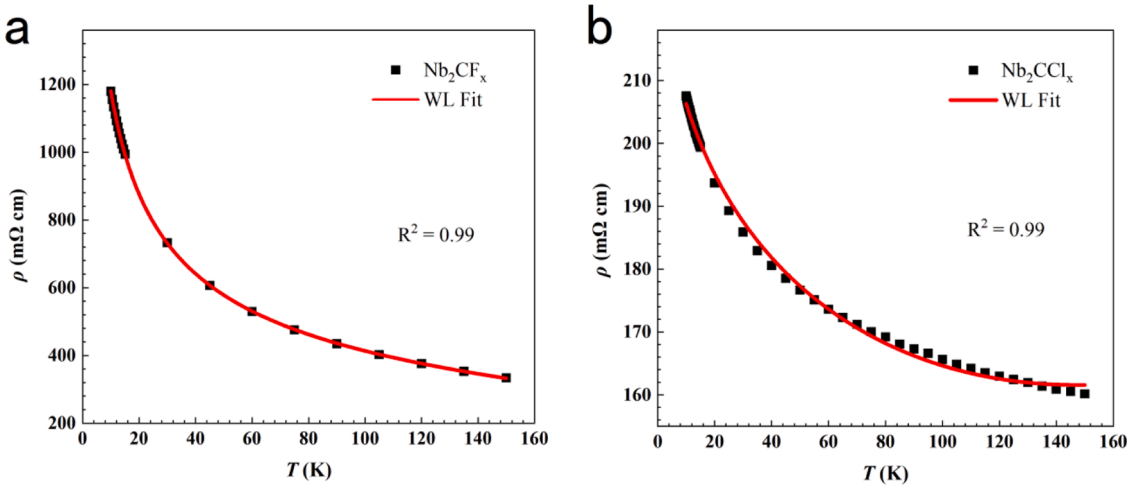

Fig. 6. The WL fitting curve of resistivity of (a) Nb_2CF_x, and (b) Nb_2CCl_x.

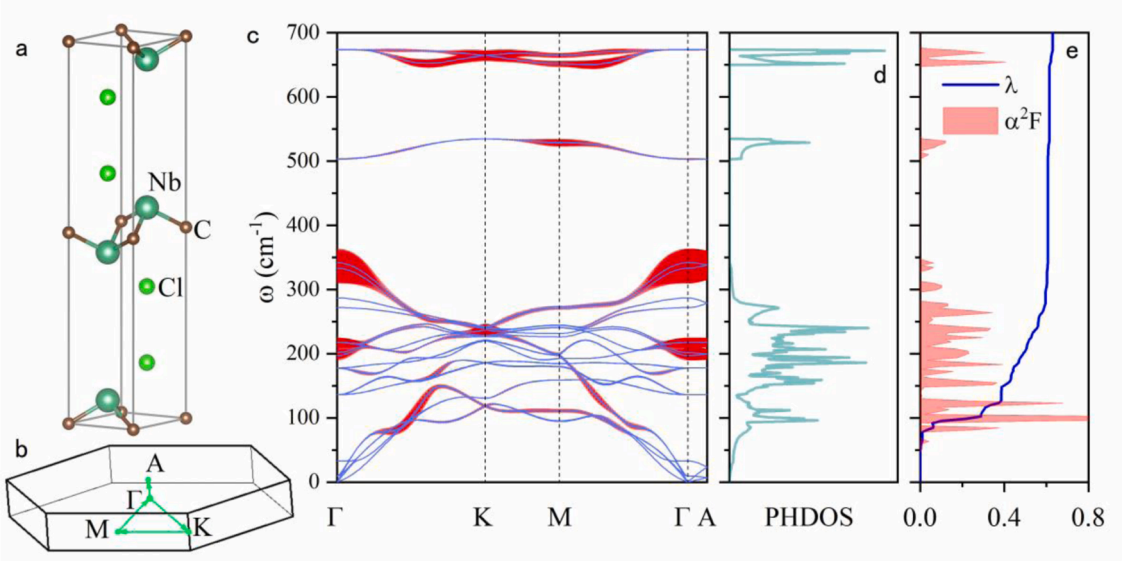

Fig. 7. (a) Crystal structure of Nb_2CCl_2 in unit cell with space group $P6_3/mmc$, (b) The first Brillouin zones, (c) Phonon dispersion with phonon linewidth $\gamma_{q\nu}$ in red bubble, (d) Phonon density of states, (e) Eliashberg function $\alpha^2F(\omega)$ and $\lambda(\omega)$.

methods. It would be highly interesting to fabricate Nb_2CF_x by the high-temperature molten salts method and examine its superconductivity. Our results clarify the inconsistencies in the current research and provide an insight into the superconductivity of MXenes materials.

CRediT authorship contribution statement

Kai Wang: Investigation, Visualization, Writing – original draft, Writing – review & editing. **Haolin Jin:** Investigation, Visualization, Writing – review & editing. **Hongye Li:** Investigation. **Zhongquan Mao:** Formal analysis. **Lingyun Tang:** Formal analysis. **Dan Huang:** Formal analysis. **Ji-Hai Liao:** Investigation, Visualization, Resources, Writing – review & editing, Funding acquisition. **Jiang Zhang:** Conceptualization, Resources, Writing – review & editing, Funding acquisition, Supervision.

Declaration of Competing Interest

We declare that we do not have any known competing financial interests or personal relationships that could have appeared to influence the work reported in this paper.

Acknowledgements

This work was supported by the Key Technologies R&D Program of Guangzhou City (No. 201704020182 and 201803030008), Guangzhou Basic and Applied Basic Research Foundation (No. 202102080166), and Open Foundation of Guangxi Key Laboratory of Processing for Non-ferrous Metals and Featured Materials, Guangxi University (No. 2021GXYSOF11).

Supplementary materials

Supplementary material associated with this article can be found, in the online version, at doi:10.1016/j.surfin.2021.101711.

References

[1] M. Naguib, M. Kurtoglu, V. Presser, J. Lu, J. Niu, M. Heon, et al., Two-dimensional nanocrystals produced by exfoliation of Ti_3AlC_2, Adv. Mater. 23 (2011) 4248–4253, https://doi.org/10.1002/adma.201102306.
[2] M. Naguib, O. Mashtalir, J. Carle, V. Presser, J. Lu, L. Hultman, et al., Two-dimensional transition metal carbides, ACS Nano 6 (2012) 1322–1331, https://doi.org/10.1021/nn204153h.

[3] B. Anasori, M.R. Lukatskaya, Y. Gogotsi, 2D metal carbides and nitrides (MXenes) for energy storage, Nat. Rev. Mater. 2 (2017) 16098, https://doi.org/10.1038/natrevmats.2016.98.

[4] H. Kim, B. Anasori, Y. Gogotsi, H.N. Alshareef, Thermoelectric properties of two-dimensional molybdenum-based MXenes, Chem. Mater. 29 (2017) 6472–6479, https://doi.org/10.1021/acs.chemmater.7b02056.

[5] J. Zhou, J. Palisaitis, J. Halim, M. Dahlqvist, Q. Tao, I. Persson, et al., Boridene: two-dimensional $Mo_{4/3}B_{2-x}$ with ordered metal vacancies obtained by chemical exfoliation, Science 373 (2021) 801–805, https://doi.org/10.1126/science.abf6239.

[6] M. Naguib, M.W. Barsoum, Y. Gogotsi, Ten years of progress in the synthesis and development of MXenes, Adv. Mater. 33 (2021), 2103393, https://doi.org/10.1002/adma.202103393.

[7] M. Naguib, J. Halim, J. Lu, K.M. Cook, L. Hultman, Y. Gogotsi, M.W. Barsoum, New two-dimensional niobium and vanadium carbides as promising materials for Li-ion batteries, J. Am. Chem. Soc. 135 (2013) 15966–15969, https://doi.org/10.1021/ja405735d.

[8] M. Khazaei, M. Arai, T. Sasaki, M. Estili, Y. Sakka, Two-dimensional molybdenum carbides: potential thermoelectric materials of the MXene family, Phys. Chem. Chem. Phys. 16 (2014) 7841–7849, https://doi.org/10.1039/C4CP00467A.

[9] C. Zhang, M. Beidaghi, M. Naguib, M.R. Lukatskaya, M.Q. Zhao, B. Dyatkin, et al., Synthesis and charge storage properties of hierarchical niobium pentoxide/carbon/niobium carbide (MXene) hybrid materials, Chem. Mater. 28 (2016) 3937–3943, https://doi.org/10.1021/acs.chemmater.6b01244.

[10] Z. Jing, H. Wang, X. Feng, B. Xiao, Y. Ding, K. Wu, et al., Superior thermoelectric performance of ordered double transition metal MXenes: $Cr_2TiC_2T_2$ (T=-OH or -F), J. Phys. Chem. Lett. 10 (2019) 5721–5728, https://doi.org/10.1021/acs.jpclett.9b01827.

[11] Y. Gogotsi, Q. Huang, MXenes: two-dimensional building blocks for future materials and devices, ACS Nano 15 (2021) 5775–5780, https://doi.org/10.1021/acsnano.1c03161.

[12] Y. Wang, R. Liu, J. Zhang, M. Miao, X. Feng, Vulcanization of Ti_3C_2T MXene/natural rubber composite films for enhanced electromagnetic interference shielding, Appl. Surf. Sci. 546 (2021), 149143, https://doi.org/10.1016/j.apsusc.2021.149143.

[13] M. Singh, A.K. Singh, Performance improvement of photovoltaic: utilization of two-dimensional $Ti_3C_2T_x$ MXene, Surf. Interfaces 27 (2021), 130656, https://doi.org/10.1016/j.surfin.2021.101566.

[14] H. Jin, K. Wang, Z. Mao, L. Tang, J. Zhang, X. Chen, The structural, magnetic, Raman and electrical transport properties of Mn intercalated $Ti_3C_2T_X$, J. Phys.: Condens. Matter 34 (2022), 015701, https://doi.org/10.1088/1361-648X/ac296f.

[15] A.M. Goldman, Superconductor–insulator transitions in the two-dimensional limit, Phys. E 18 (2003) 1–6, https://doi.org/10.1016/S1386-9477(02)00932-3.

[16] C. Xu, L. Wang, Z. Liu, L. Chen, J. Guo, N. Kang, et al., Large-area high-quality 2D ultrathin Mo_2C superconducting crystals, Nat. Mater. 14 (2015) 1135–1141, https://doi.org/10.1038/nmat4374.

[17] J. Lei, A. Kutana, B.I. Yakobson, Predicting stable phase monolayer Mo_2C (MXene), a superconductor with chemically-tunable critical temperature, J. Mater. Chem. C 5 (2017) 3438–3444, https://doi.org/10.1039/C7TC00789B.

[18] T.H. Scabarozi, J. Roche, A. Rosenfeld, S.H. Lim, L. Salamanca-Riba, G. Yong, et al., Synthesis and characterization of Nb_2AlC thin films, Thin Solid Films 517 (2009) 2920–2923, https://doi.org/10.1016/j.tsf.2008.12.047.

[19] S. Kuchida, T. Muranaka, K. Kawashima, K. Inoue, M. Yoshikawa, J. Akimitsu, Superconductivity in Lu_2SnC, Phys. C Supercond. 494 (2013) 77–79, https://doi.org/10.1016/j.physc.2013.04.050. C.

[20] A.D. Bortolozo, Z. Fisk, O.H. Sant'Anna, C.A.M. dos Santos, A.J.S. Machado, Superconductivity in Nb_2InC, Phys. C Supercond. 469 (2009) 256–258, https://doi.org/10.1016/j.physc.2009.02.005. C.

[21] V. Kamysbayev, A.S. Filatov, H. Hu, X. Rui, F. Lagunas, D. Wang, R.F. Klie, et al., Covalent surface modifications and superconductivity of two-dimensional metal carbide MXenes, Science 369 (2020) 979–983, https://doi.org/10.1126/science.aba8311.

[22] Z.U.D. Babar, M.S. Anwar, M. Mumtaz, M. Iqbal, R.K. Zheng, D. Akinwande, et al., Peculiar magnetic behaviour and Meissner effect in two-dimensional layered Nb_2C MXene, 2D Mater. 7 (2020), 035012, https://doi.org/10.1088/2053-1583/ab86d2.

[23] Z.U. Din Babar, J. Fatheema, N. Arif, M.S. Anwar, S. Gul, M. Iqbal, et al., Magnetic phase transition from paramagnetic in Nb_2AlC-MAX to superconductivity-like diamagnetic in Nb_2C-MXene: an experimental and computational analysis, RSC Adv. 10 (2020) 25669–25678, https://doi.org/10.1039/D0RA04568C.

[24] J. Halim, I. Persson, E.J. Moon, P. Kühne, V. Darakchieva, P.O.Å. Persson, et al., Electronic and optical characterization of 2D Ti_2C and Nb_2C (MXene) thin films, J. Phys. Condens. Matter 31 (2019), 165301, https://doi.org/10.1088/1361-648X/ab00a2.

[25] J. Bekaert, C. Sevik, M.V. Milošević, First-principles exploration of superconductivity in MXenes, Nanoscale 12 (2020) 17354–17361, https://doi.org/10.1039/D0NR03875J.

[26] Y. Yang, C.S. Ting, Electronic structures and electron–phonon superconductivity of Nb_2C-based MXenes, J. Phys. D Appl. Phys. 53 (2020), 485301, https://doi.org/10.1088/1361-6463/aba21b.

[27] M. Ghidiu, M.R. Lukatskaya, M.Q. Zhao, Y. Gogotsi, M.W. Barsoum, Conductive two-dimensional titanium carbide 'clay' with high volumetric capacitance, Nature 516 (2014) 78–81, https://doi.org/10.1038/nature13970.

[28] P. Giannozzi, S. Baroni, N. Bonini, M. Calandra, R. Car, C. Cavazzoni, et al., QUANTUM ESPRESSO: a modular and open-source software project for quantum simulations of materials, J. Phys. Condens. Matter 21 (2009), 395502, https://doi.org/10.1088/0953-8984/21/39/395502.

[29] G. Prandini, A. Marrazzo, I.E. Castelli, N. Mounet, N. Marzari, Precision and efficiency in solid-state pseudopotential calculations, npj Comput. Mater. 4 (2018) 72, https://doi.org/10.1038/s41524-018-0127-2.

[30] A. Dal Corso, Pseudopotentials periodic table: from H to Pu, Comput. Mater. Sci. 95 (2014) 337–350, https://doi.org/10.1016/j.commatsci.2014.07.043.

[31] M. Methfessel, A.T. Paxton, High-precision sampling for Brillouin-zone integration in metals, Phys. Rev. B 40 (1989) 3616–3621, https://doi.org/10.1103/PhysRevB.40.3616.

[32] A.C. Rose-Innes, E.H. Rhoderick, Introduction to Superconductivity, 2nd ed., Pergamon, Oxford, 1978.

[33] J.L. Hart, K. Hantanasirisakul, A.C. Lang, B. Anasori, D. Pinto, Y. Pivak, et al., Control of MXenes' electronic properties through termination and intercalation, Nat. Commun. 10 (2019) 522, https://doi.org/10.1038/s41467-018-08169-8.

[34] K. Zhang, M. Di, L. Fu, Y. Deng, Y. Du, N. Tang, Enhancing the magnetism of 2D carbide MXene Ti_3C_2Tx by H_2 annealing, Carbon 157 (2020) 90–96, https://doi.org/10.1016/j.carbon.2019.10.016. N Y.

[35] P.A. Lee, T.V. Ramakrishnan, Disordered electronic systems, Rev. Mod. Phys. 57 (1985) 287–337, https://doi.org/10.1103/RevModPhys.57.287.

[36] Y.J. Kim, K.J. Chang, Weak localization effect in superconductors, Mod. Phys. Lett. B 12 (1998) 763–773, https://doi.org/10.1142/S0217984998000895.

[37] G. Herranz, F. Sánchez, B. Martínez, J. Fontcuberta, M.V. García-Cuenca, C. Ferrater, M. Varela, et al., Weak localization effects in some metallic perovskites, Eur. Phys. J. B 40 (2004) 439–444, https://doi.org/10.1140/epjb/e2004-00207-9.

[38] J. Biscaras, N. Bergeal, A. Kushwaha, T. Wolf, A. Rastogi, R.C. Budhani, et al., Two-dimensional superconductivity at a Mott insulator/band insulator interface $LaTiO_3/SrTiO_3$, Nat. Commun. 1 (2010) 89, https://doi.org/10.1038/ncomms1084.

[39] K. Górnicka, X. Gui, B. Wiendlocha, L.T. Nguyen, W. Xie, R.J. Cava, et al., $NbIr_2B_2$ and $TaIr_2B_2$-new low symmetry noncentrosymmetric superconductors with strong spin-orbit coupling, Adv. Funct. Mater. 31 (2021), 2007960, https://doi.org/10.1002/adfm.202007960.

[40] Z.U.D. Babar, R.K. Zheng, M. Mumtaz, S. Rizwan, Magneto-transport of mechanically-pressed niobium carbide (Nb_2C) distorted MXene, Mater. Lett. 285 (2021), 129210, https://doi.org/10.1016/j.matlet.2020.129210.

[41] G. Herranz, B. Martínez, J. Fontcuberta, F. Sánchez, C. Ferrater, M.V. García-Cuenca, et al., Enhanced electron-electron correlations in nanometric $SrRuO_3$ epitaxial films, Phys. Rev. B 67 (2003), 174423, https://doi.org/10.1103/PhysRevB.67.174423.

[42] V. Sadovskii, Superconductivity and localization, Phys. Rep. 282 (1997) 225.

[43] L. Li, Y.M. Gan, Z.H. Lu, X. Yu, S. Qing, Z. Gao, R. Zhang, G. Feng, The effects of Fe, Co and Ni doping in $CuAl_2O_4$ spinel surface and bulk: a DFT study, Appl. Surf. Sci. 521 (2020), 146478, https://doi.org/10.1016/j.apsusc.2020.146478.

[44] L. Shi, Y. Huang, Z.H. Lu, W. Cen, X. Yu, S. Qing, Z. Gao, R. Zhang, G. Feng, Surface property of the Cu doped γ-Al_2O_3: a density functional theory study, Appl. Surf. Sci. 535 (2021), 147651, https://doi.org/10.1016/j.apsusc.2020.147651.

[45] L. Shi, S. Meng, S. Jungsuttiwong, S. Namuangruk, Z.H. Lu, L. Li, R. Zhang, G. Feng, S. Qing, Z. Gao, X. Yu, High coverage H_2O adsorption on $CuAl_2O_4$ surface: a DFT study, Appl. Surf. Sci. 507 (2020), 145162, https://doi.org/10.1016/j.apsusc.2019.145162.

[46] L. Shi, D. Wang, X. Yu, L. Li, Z.H. Lu, G. Feng, R. Zhang, S. Qing, Z. Gao, Q. Luo, Adsorption of Cun (n = 1–4) clusters on $CuAl_2O_4$ spinel surface: a DFT study, Mol. Catal. 468 (2019) 29–35, https://doi.org/10.1016/j.mcat.2019.02.009.

[47] P.B. Allen, R.C. Dynes, Transition temperature of strong-coupled superconductors reanalyzed, Phys. Rev. B 12 (1975) 905–922, https://doi.org/10.1103/PhysRevB.12.905.

[48] Y. Zhao, S. Zeng, J. Ni, Phonon-mediated superconductivity in borophenes, Appl. Phys. Lett. 108 (2016), 242601, https://doi.org/10.1063/1.4953775.

[49] J.J. Zhang, B. Gao, S. Dong, Strain-enhanced superconductivity of MoX_2 (X = S or Se) bilayers with Na intercalation, Phys. Rev. B 93 (2016), 155430, https://doi.org/10.1103/PhysRevB.93.155430.

[50] S. Zeng, Y. Zhao, G. Li, J. Ni, Strongly enhanced superconductivity in doped monolayer MoS_2 by strain, Phys. Rev. B 94 (2016), 024501, https://doi.org/10.1103/PhysRevB.94.024501.

[51] J.H. Liao, Y.C. Zhao, Y.J. Zhao, H. Xu, X.B. Yang, Phonon-mediated superconductivity in Mg intercalated bilayer borophenes, Phys. Chem. Chem. Phys. 19 (2017) 29237–29243, https://doi.org/10.1039/C7CP06180C.

[52] Y. Zhao, S. Zeng, C. Lian, Z. Dai, S. Meng, J. Ni, Multigap anisotropic superconductivity in borophenes, Phys. Rev. B 98 (2018), 134514, https://doi.org/10.1103/PhysRevB.98.134514.

[53] Y. Sun, J. Lv, Y. Xie, H. Liu, Y. Ma, Route to a superconducting phase above room temperature in electron-doped hydride compounds under high pressure, Phys. Rev. Lett. 123 (2019), 097001, https://doi.org/10.1103/PhysRevLett.123.097001.

[54] T. Bo, P.F. Liu, L. Yan, B.T. Wang, Electron-phonon coupling superconductivity in two-dimensional orthorhombic MB_6 (M = Mg, Ca, Ti, Y) and hexagonal MB_6 (M = Mg, Ca, Sc, Ti), Phys. Rev. Mater. 4 (2020), 114802, https://doi.org/10.1103/PhysRevMaterials.4.114802.